Bull. Mater. Sci., Vol. 37, No. 5, August 2014, pp. 953–961. © Indian Academy of Sciences.

Size-dependent magnetic properties in $Cu_{0.25}Co_{0.25}Zn_{0.5}Fe_2O_4$

HINA BHARGAVA[1], V D SUDHEESH[2], J NEHRA[2], VARKEY SEBASTIAN[3], N LAKSHMI[2,*], K VENUGOPALAN[2], V R REDDY[4] and AJAY GUPTA[4]

[1]Department of Physics, Vijaya College, Bangalore 560 004, India
[2]Department of Physics, Mohanlal Sukhadia University, Udaipur 313 001, India
[3]Department of Physics, Nirmalagiri College, Kuthuparamba 670 701, India
[4]UGC-DAE Consortium for Scientific Research, Khandwa Road, Indore 452 001, India

MS received 12 September 2013; revised 12 November 2013

Abstract. **$Cu_{0.25}Co_{0.25}Zn_{0.5}Fe_2O_4$ nanoparticles were prepared by a co-precipitation method and the size was varied by varying annealing temperatures. The cation distribution, estimated using Mössbauer spectroscopy, shows that it is the same for all samples, irrespective of the size. The variation of Curie temperature and saturation magnetization as a function of particle size, studied using d.c. magnetization, clearly indicates that these are a result of finite size scaling effects. The superparamagnetic size limit is estimated to be 8 nm.**

Keywords. **Co-precipitation; magnetic properties; finite-size scaling.**

1. Introduction

Nanoparticles exhibit unusual properties that are technologically important and remarkably different from that of their bulk counterparts (Gajbhiye *et al* 2002; Hassnain *et al* 2010; Thakur *et al* 2012; Šutka *et al* 2013). At the nanoscale, the surface-to-volume ratio of atoms becomes large and surface effects become more dominant (Kihal *et al* 2012). Hence, bulk properties may give way to surface properties and/or be significantly perturbed by the surface (Lima *et al* 2010; Vázquez *et al* 2010). Moreover, the large surface fraction opens up the opportunity for manipulation of properties via interfacial interactions (Lakshmi *et al* 2009). Knowledge of these fundamental properties is essential for creative use of nanoparticles in important technical applications (Dennis *et al* 2009).

For example, superparamagnetic properties of magnetic nanoparticles provide opportunities in potential applications such as ferrofluid technology, magnetocaloric refrigeration, contrast enhancement in magnetic resonance imaging and magnetically guided drug delivery (Ai and Jiang 2010; Hu *et al* 2011; Jeun *et al* 2012). The possibility of using the superparamagnetic properties of metallic systems like Fe, Co and Ni for such applications has been extensively studied. However, chemical instability of these metallic nanosystems allow only limited applications. Magnetic metal oxides, which can be prepared through chemical methods and are chemically more stable, offer great opportunities for developing superparamagnetic nanoparticles with desirable properties.

In nanoparticles of magnetic metal oxides such as ferrites, a strong decrease in saturation magnetization, M_s, and an enhancement of coercivity, H_c, as compared to the bulk materials, have been reported (Yamamoto and Makino 1994; Kodama *et al* 1996). These phenomena have been explained by assuming the existence of random canting of surface spins, pinning of spins at particle surface (Coey 1971; Coey and Khalafella 1972) or the presence of a dead layer around the magnetic core material (Berkowitz *et al* 1968). In addition to these surface effects, interparticle interactions may also explain the interesting properties exhibited by nanoparticles (García *et al* 1999; Mørup *et al* 2010; Hiroi *et al* 2011).

Cobalt ferrite ($CoFe_2O_4$) promises to be a good candidate for diverse applications ranging from biological applications as in magnetic drug delivery to magnetic recording applications such as audio and videotape and high-density digital recording discs due to a combination of high magnetocrystalline anisotropy and good chemical stability. Partial substitution of Co with other cations allows a systematic variation of magnetic properties. Thus, the mixed spinel $Co_{0.5}Zn_{0.5}Fe_2O_4$ is well suited for the study of the effect of initial preparation conditions on the cation distribution and substitution effects since Co has a strong preference for octahedral sites and Zn, a strong preference for the tetrahedral sites. Partial replacement of Co with Cu into nano-sized $Co_{0.5}Zn_{0.5}Fe_2O_4$ is also expected to affect the magnetic properties considerably due to distortion produced in the spinel structure, since Cu acts as a Jahn–Teller cation and also because of its ease of occupancy of either of the two available (tetrahedral or octahedral) sites. For example, recent studies on nano-sized Cu–Co–Zn ferrite show that it has great

*Author for correspondence (nambakkat@yahoo.com)

potential as a magnetic recording media (Sindhu and Birajdar 2013). In this paper, the possibility of tailoring the magnetic properties of $Cu_{0.25}Co_{0.25}Zn_{0.5}Fe_2O_4$ by controlling the particle sizes through annealing temperature is investigated. The samples are prepared by the versatile chemical co-precipitation method and annealed at different temperatures to obtain nanoparticles of different sizes. Structural and magnetic characterization of the particles is done using X-ray diffraction (XRD) and vibrating sample magnetometry, respectively.

2. Experimental

Nanoparticles of $Cu_{0.25}Co_{0.25}Zn_{0.5}Fe_2O_4$ were prepared by a chemical co-precipitation method using analytical grade $CuCl_2{\cdot}2H_2O$, $CoCl_2{\cdot}6H_2O$, $ZnCl_2$ and $Fe(NO_3)_3{\cdot}9H_2O$. The salts were taken in stoichiometric ratios and then dissolved in water maintained at 333 K temperature. During precipitation, the pH was maintained at 10 using 25% ammonia solution. The precipitate was stirred at 333 K for 2 h and, then, stirred at 368 K for 1 h to complete the digestion. The precipitate was then washed several times and dried by heating at 373 K for 24 h. The dried precipitate was then divided into six equal parts and annealed at 573, 673, 773, 873, 973 and 1073 K, respectively, for 24 h.

Structural characterization and determination of the average sizes of nano-sized samples were done using XRD spectra obtained on a Rigaku-Miniflex X-ray diffractometer with CuKα radiation. Mössbauer spectra room temperature (RT) were recorded using a standard Austin drive and controller assembly in the constant acceleration mode with a 12 mCi ^{57}Co(Rh) source. Velocity calibration was done using metallic iron foil. Low-temperature Mössbauer spectra were obtained at 20 K using a closed cycled refrigerator assembly. Magnetic measurements were done using a Lake Shore 304 vibrating sample magnetometer (VSM). For low and high temperatures *M–T* measurements, a small field of 4 kA/m was used.

3. Results and discussion

3.1 *Structural analysis*

XRD patterns of all samples of $Cu_{0.25}Co_{0.25}Zn_{0.5}Fe_2O_4$ annealed at different temperatures from 573 to 1073 K are shown in figure 1. All samples exhibit peaks indicative of the single-phase spinel structure. The increase in the sharpness of XRD peaks with increase in the annealing temperature indicates increased crystallinity. Average particle sizes of the samples were estimated using the Scherrer equation which show that the crystallite size increases from 3 to 40 nm, when the annealing temperature is varied from 573 to 1073 K. The crystallite size, along with other structural parameters, is listed in table 1 and the trend in particle size with annealing temperature is shown in figure 2.

On annealing, two or more particles fuse together by melting their surfaces. It is interesting to note that the particles' surfaces are melted well below the melting point of their bulk form. This is because in nano-sized materials, a large fraction of atoms is present at the boundaries. These atoms are weakly bound, enhancing their diffusivity and leading to a sharp decrease of the surface melting point of the particles (Kumar *et al* 2008).

The values of lattice constant of the samples calculated from the peak positions are given in table 1. It is seen that the lattice constant initially decreases and then increases linearly for annealing temperatures ≥ 773 K. The initial decrease in the lattice constant as a function of particle size can be understood as follows. When the number of atoms in an isolated particle is reduced, the excess free energy associated with the surface constitutes an increasingly important fraction of the particle's total free energy. A small particle can reduce this excess free energy by changing its lattice structure in an appropriate manner. This reduction in the excess free energy is accompanied by the conversion of the lattice to an energetically less favourable crystallographic structure; however, the overall energetics increase the stability. A different approach is based on the surface stresses resulting in a hydrostatic pressure on the particle of reduced size. This leads to the crystallographic phase associated with the high pressure (Upadhyay 2003). When the annealing temperature is increased to 773 K or more, the particle size increases and the surface-to-volume ratio decreases. This leads to an increase in the distortion of the spinel structure due to the cooperative Jahn–Teller effect arising from the octahedral cupric ions (Tailhades *et al* 1998). At higher annealing temperatures, the distortion

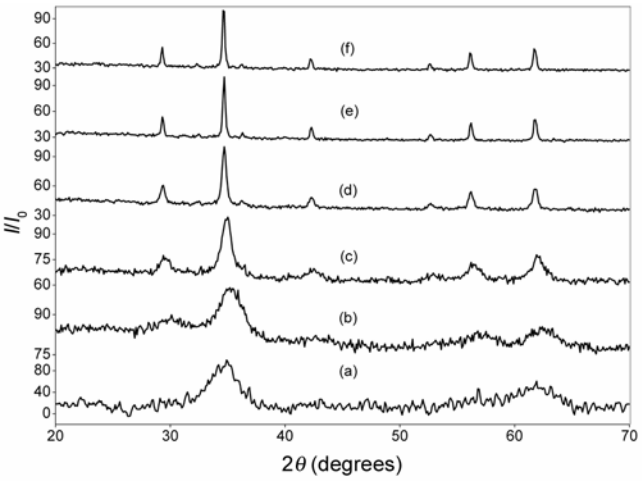

Figure 1. X-ray diffraction patterns of $Cu_{0.25}Co_{0.25}Zn_{0.5}Fe_2O_4$ annealed at (**a**) 573, (**b**) 673, (**c**) 773, (**d**) 873, (**e**) 973 and (**f**) 1073 K.

Table 1. Obtained structural parameters for $Cu_{0·25}Co_{0·25}Zn_{0·5}Fe_2O_4$ annealed at different temperatures ranging from 573 to 1073 K.

Annealing temperature (K)	Particle size (nm)	Lattice constant (Å)	X-ray density (g/cm^3)	Measured density (g/cm^3)	Porosity (%)
573	3	8·472	5·22	2·15	58
673	4	8·448	5·27	3·18	39
773	8	8·433	5·29	3·72	29
873	19	8·444	5·27	4·03	23
973	33	8·447	5·27	4·44	15
1073	40	8·457	5·25	5·12	2

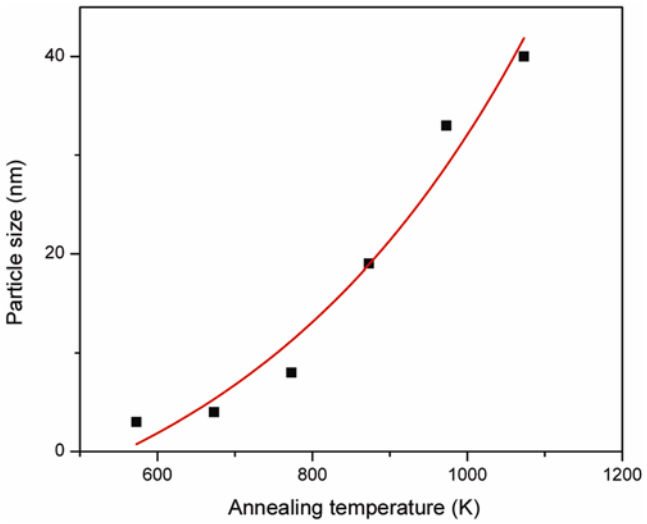

Figure 2. Variation of particle size with annealing temperature. The red line is a sigmoidal fit to experimental points.

increases and the lattice constant shows an increase with annealing temperature.

3.2 *Mössbauer analysis*

RT Mössbauer spectra have been recorded for samples annealed at different temperatures and RT Mössbauer spectra of samples annealed at the lowest and highest temperatures, i.e. at 573 and 1073 K, are given in figure 3. RT Mössbauer spectra of samples annealed at 573 and 673 K are clear doublets without the presence of any sextets, indicating that these samples are superparamagnetic at RT, while that of sample annealed at 773 K exhibits the coexistence of superparamagnetic doublets along with a relaxation component. Mössbauer spectra of samples annealed at 873, 973 and 1073 K show the presence of well-resolved sextets and a relaxation component due to particle size distribution. The smaller particles contribute to the relaxation spectra, while the bigger ones give rise to resolved sextets. The spectra of samples annealed at 873, 973 and 1073 K have, therefore, been fitted with two discrete sextets corresponding to the tetragonal A and octahedral B sites with hyperfine fields of about 35 and 40 T, respectively, for all samples along with a relaxation component. The hyperfine parameters obtained by fitting the spectra are tabulated in table 2 and cation distribution for samples annealed at 873, 973 and 1073 K which corresponds to $(Zn_{0·5}Fe_{0·5})^A[Cu_{0·25}Co_{0·25}Fe_{1·5}]^B$ are given in table 3. To obtain the cation distribution of particles which are superparamagnetic at RT, low-temperature (LT) Mössbauer spectra of the sample annealed at 573 K has been taken at 20 K (figure 4). Keeping this in mind, results obtained from the RT Mössbauer spectrum of sample annealed at 573 K, initially two broad sextets with hyperfine fields of 45·5 and 47 T have been fitted to the LT spectrum, which defines the average hyperfine fields at Fe in the tetrahedral A and octahedral B sites. However, the individual line widths are much broader than in the case of the RT spectra, and a careful examination of the LT spectrum shows a definite asymmetry in the peaks. The LT spectrum has, therefore, been re-fitted for four unique sites corresponding to one A and three B sites designated as B1, B2 and B3.

It has generally been observed that in spinel ferrites, the sextet due to Fe at the B site is much broader than that at the A site and is due to the possibility of more than one B sites (Sawatzky *et al* 1969), because of the random distribution of cations, when more than one cation occupies a particular site. In the present system, four cations–iron, copper, cobalt and zinc—are present and so at any one particular site, the distribution of these cations is in a random fashion, with Zn having a very strong preference for the A site and Cu and Co preferring the B site. Fe does not have a very strong preference for either sites with a greater probability of occupancy of the B site. This leads to a probability of finding several A/B sites. In ferrites, arrangement of cations at the A site affects the hyperfine fields at the B site and vice versa, since the magnetic interaction between these sites is of the superexchange type, mediated by oxygen ions. Although such a random distribution of cations can occur at both the sites, the B site is more affected by the difference that occurs in the cation distribution at the A site. This is so because the B site has six A sites as nearest neighbours, whereas the A site has twelve B sites as nearest neighbours and so the possibility of formation of more than one distinct A site is 1/12th that of the B

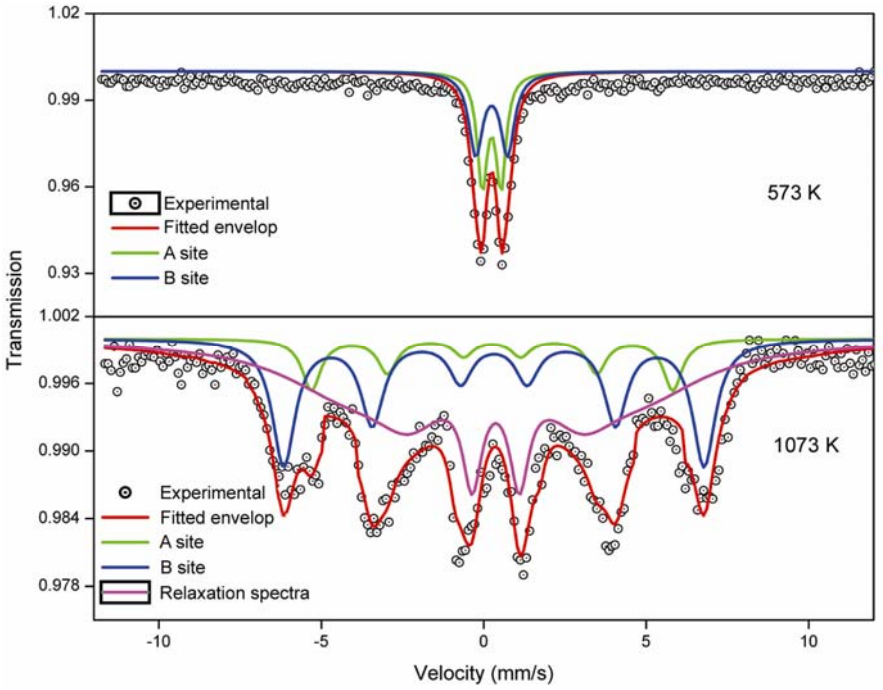

Figure 3. Room temperature Mössbauer spectra for samples annealed at 573 and 800 K.

Table 2. Parameters obtained from fitting room temperature Mössbauer spectra for samples annealed at 573, 673, 773, 873, 973 and 1073 K.

Annealing temperature (K)	Isomer shift (mm/s) (± 0·04 mm/s)			Hyperfine field (T) (± 0·3 T)		
	A site	B site	Relaxation spectra	A site	B site	Relaxation spectra
573	0·24	0·24		Superparamagnetic		
673	0·29	0·29		Superparamagnetic		
773	0·23	0·25	0·28	Superparamagnetic		13·71
873	0·25	0·28	0·26	34·52	38·89	31·22
973	0·25	0·26	0·29	34·53	40·15	33·18
1073	0·25	0·25	0·36	34·46	40·08	28·38

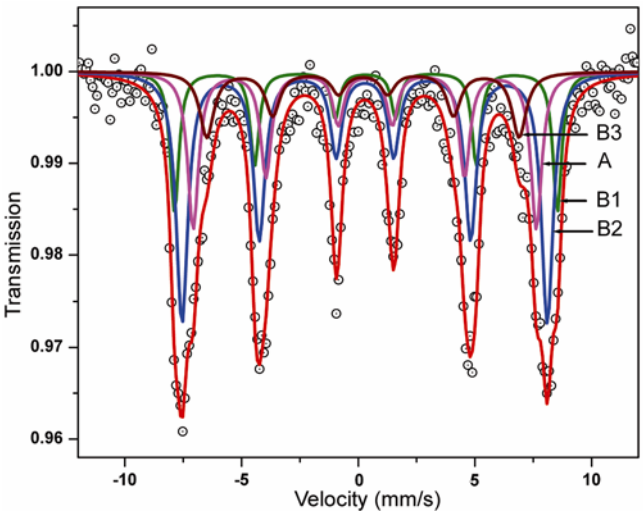

Figure 4. Low temperature (20 K) Mössbauer spectrum of sample annealed at 573 K.

Table 3. Cation distribution of samples annealed at different temperatures obtained by Mössbauer analysis.

Annealing temperature (K)	Cation distribution
873	$(Zn_{0·5}Fe_{0·5})^{A}[Cu_{0·25}Co_{0·25}Fe_{1·5}]^{B}$
973	$(Zn_{0·5}Fe_{0·5})^{A}[Cu_{0·25}Co_{0·25}Fe_{1·5}]^{B}$
1073	$(Zn_{0·5}Fe_{0·5})^{A}[Cu_{0·25}Co_{0·25}Fe_{1·5}]^{B}$

site (Krieble *et al* 2005). Accordingly, the LT Mössbauer spectrum for the sample annealed at 573 K has been fitted for a unique A site and three different B sites. However, since it is not possible to assign individual cation distributions for the B1, B2 and B3 sites, the cation distribution in this sample has been calculated from the total area under the curve occupied by all the B sites and the cation distribution at the B site given in table 4 is an average

Table 4. Parameters obtained from fitting LT (20 K) Mössbauer spectrum of $Cu_{0·25}Co_{0·25}Zn_{0·5}Fe_2O_4$ annealed at 573 K.

Site	Isomer shift ± 0·04 (mm/s)	Hyperfine field ± 0·03 (*T*)	Width ± 0·04 (mm/s)	Cation distribution
A	0·29	45·5	0·56	$(Zn_{0·5}Fe_{0·5})^A[Cu_{0·25}Co_{0·25}Fe_{1.5}]^B$
B1	0·31	50·8	0·45	
B2	0·28	48·5	0·60	
B3	0·28	41·5	0·73	

Table 5. D.C. magnetization parameters for $Cu_{0·25}Co_{0·25}Zn_{0·5}Fe_2O_4$ annealed at temperatures ranging from 573 to 1073 K.

Annealing temperature (K)	Saturation magnetization (Am^2/kg)	Coercivity (kA/m)	Magnetic particles size (nm)	*t*/*D* (%)
573	5·2	SPM	2	15·7
673	18	SPM	3	13·2
773	37·8	SPM	6	9·5
873	54·7	5·25	16	6·4
973	64·1	6·45	30	4·6
1073	68·4	4·78	37	3·8

over the three discrete sites and is found to be the same as for samples annealed at 873, 973 and 1073 K.

3.3 *D.C. magnetization*

The field-dependent magnetization (*M–H* curve) of $Cu_{0·25}Co_{0·25}Zn_{0·5}Fe_2O_4$, annealed at different temperatures, i.e. 573, 673, 773, 873, 973 and 1073 K, are shown in figure 5. *M–H* curves for samples annealed at 573, 673 and 773 K, having particle sizes of 3, 4 and 8 nm, respectively, show reversible behaviour (figure 5). This reversible behaviour indicates the superparamagnetic nature of these samples. However, the *M–H* curves for samples annealed at 873, 973 and 1073 K with particle size of 19, 33 and 40 nm, respectively, clearly display hysteresis and indicate the ferrimagnetic nature of the particles.

Saturation magnetization, M_S, of the samples annealed at temperatures ranging from 573 to 1073 K, estimated by plotting *M* vs 1/*H* for 1/*H* tends to zero, shows a decrease with increase in particle size (table 5). This decrease in the saturation magnetization of nano-sized samples is explained by the presence of a magnetically dead layer at the surface of the particles (Gajbhiye *et al* 2002). Tang *et al* (1991) derived an empirical relation for size-dependent saturation magnetization as

$$M_S = M_B\left(1-\frac{6t}{D}\right), \tag{1}$$

where M_S is the saturation magnetization of the sample, M_B is the saturation magnetization of the corresponding bulk sample, *D* the particle size and *t* the thickness of the magnetically dead layer.

Saturation magnetization (M_S) of bulk $Cu_{0·25}Co_{0·25}Zn_{0·5}Fe_2O_4$ has been estimated by plotting saturation magnetization of samples annealed at 573 to 1073 K with the inverse of the particles size (D^{-1}). By using this value of M_B and the observed values of M_s for different particle sizes, the thickness of the magnetically dead layer has been estimated (table 5).

Magnetic particle size of samples annealed at different temperatures ranging from 573 to 1073 K (particle size ranging from 3 to 40 nm) has been determined by excluding the thickness of the magnetically dead layer. As the annealing temperature (particle size) increases, the magnetic particle size increases at the expense of magnetically dead layer (table 5). Due to decrease in the volume percent of the magnetically dead layer, the saturation magnetization of $Cu_{0·25}Co_{0·25}Zn_{0·5}Fe_2O_4$ increases with increase in the annealing temperature (particle size). The plot of the variation of M_s with particle size (figure 6) shows that the increase in M_s is sigmoidal in nature. This is because for the same cation distribution, the volume percent of the magnetically dead layer becomes so less with increase in particle size, so as to not affect the value of M_s any further.

The presence of magnetically dead layer also affects the anisotropy of the samples. The effective anisotropy is given by

$$K_{eff} = K + K_S + K_{sh} + K_{in}, \tag{2}$$

where *K* is the magnetocrystalline anisotropy, K_S a constant of surface anisotropy, K_{sh} the shape anisotropy constant and K_{in} the constant of supplementary anisotropy that reflects inter-particle interactions (Caizer and Stefanescu 2002). It is evident from table 5 that the volume fraction of the surface of the magnetically dead layer increases as the particle size decreases. Due to this increase in the surface of magnetically dead layer, the contribution of surface anisotropy to K_{eff} increases, which

leads to an increase in the effective anisotropy constant, K_{eff}, with decreasing particle size.

Coercivity (H_C) of the ferrimagnetic samples, annealed at 873, 973 and 1073 K, initially increases and then decreases. The sample annealed at 973 K has the highest coercivity, with an H_C value of 6·45 kA/m (table 5), indicating that at this temperature, the particle size is approximately equal to the single domain size. The decrease in H_C beyond 973 K is attributed to particles exceeding single-domain particle size and becoming multi-domain due to annealing. Thus, the sample annealed at 1073 K is multi-domained and has a number of domain walls (Chinnasamy *et al* 2003; Andrés Vergés *et al* 2008). The magnetization/demagnetization caused by domain wall movement requires less energy than that required by single domain rotation. As the number of walls increases with particle size or annealing temperature, the contribution of wall movement to magnetization or demagnetization is greater than that of single domain rotation. Therefore, the particles annealed at higher temperatures have lower coercivity (Costa *et al* 2003). The lower value of coercivity of the sample annealed at 873 K can be attributed to a particle size distribution in the sample, with the smallest particles being superparamagnetic. At lower annealing temperatures, the particle sizes are smaller and tend to reach the superparamagnetic size. When the particles reach the superparamagnetic size, the energy barrier separating the two energetically degenerate magnetic orientations is small. Thus, at any temperature, the thermal activation is enough to switch the magnetic orientation. Hence, the coercivity vanishes at this particle size (Roy *et al* 2004).

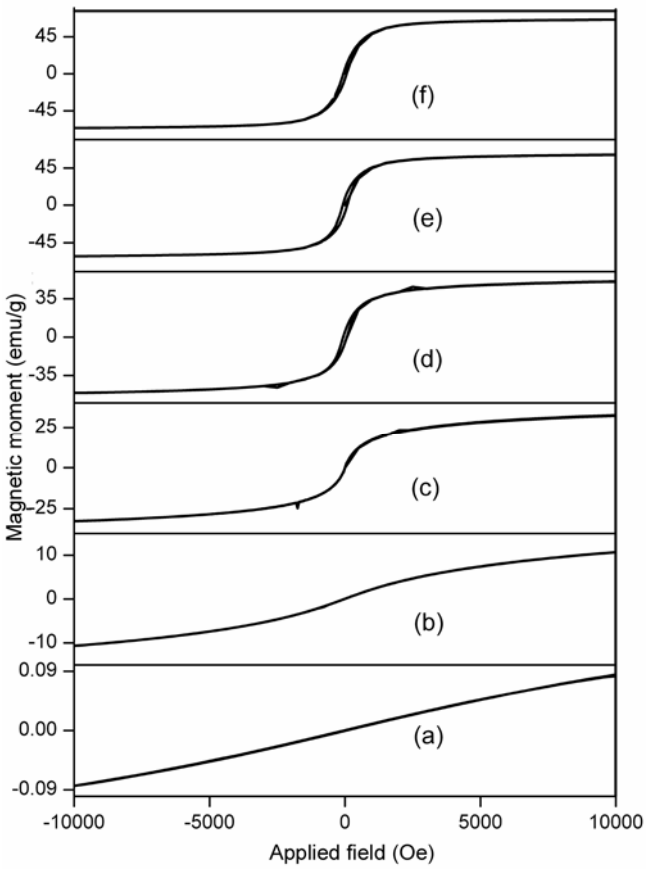

Figure 5. Room temperature *M–H* measurement for $Cu_{0·25}Co_{0·25}Zn_{0·5}Fe_2O_4$ annealed at (**a**) 573, (**b**) 673, (**c**) 773, (**d**) 873, (**e**) 973 and (**f**) 1073 K.

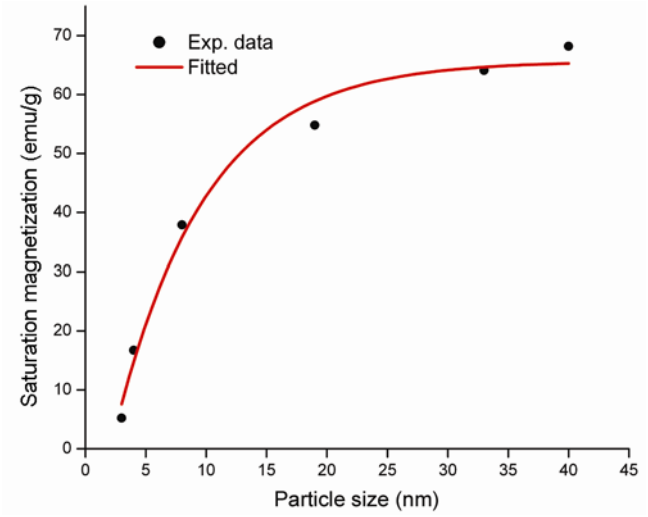

Figure 6. Variation of saturation magnetization with particle size. The red line is a sigmoidal fit to experimental points.

Field cooled–zero field cooled *M–T* measurements are commonly used to determine blocking temperature (T_B) of a magnetic material exhibiting superparamagnetism at room temperature. In zero field cooling (ZFC), the sample is first cooled from room temperature to a low temperature, well below its blocking temperature, in zero applied magnetic field. Then, a small magnetic field is applied and the magnetic moment M_{ZFC} of the sample is recorded as the temperature is increased to 300 K. For field cooled (FC) curve, the process is repeated except that the initial cooling is done in the presence of a small applied field (the field is kept the same in the warming cycle of ZFC and cooling/warming cycles of FC).

For $Cu_{0·25}Co_{0·25}Zn_{0·5}Fe_2O_4$, annealed at 573 and 673 K (particle size 3 and 4 nm, respectively), the M_{ZFC} values at first increase with decreasing temperature, reaches a maximum at the blocking temperature, T_B (85 K for 3 nm particles and 125 K for 4 nm particles), and then decreases as the temperature is further decreased (figure 7). M_{FC} values replicate the behaviour of M_{ZFC} values up to T_{irr} (100 K for 3 nm particles and 143 K for 4 nm particles). On further cooling, the FC curve deviates from the ZFC curve and the difference between the two curves increases with decreasing temperature. Blocking temperature, T_B, of $Cu_{0·25}Co_{0·25}Zn_{0·5}Fe_2O_4$ annealed at 773 K (with particle size 8 nm) is 294 K and the bifurcation temperature T_{irr} is 300 K. In this case, the ZFC curve is broad. The broadening of ZFC curve usually indicates a certain particle size

distribution, where a fraction of larger particles has already frozen at T_{irr} with the majority fraction of nanoparticles being blocked at T_B, resulting in the distribution of blocking temperatures (Sharma *et al* 2008; Choudhari *et al* 2009).

In all the three samples, M_{FC} shows an increase with decreasing temperature below T_B with a tendency towards saturation rather than a monotonically increasing behaviour, as in the case of non-interacting superparamagnetic particles. Such a behaviour is typical of systems where inter-particle interactions are present (Tiwari and Rajeev 2005).

Curie temperatures (T_C) of the samples annealed at 773, 873, 973 and 1073 K are determined from high-temperature M–T measurements at a small field of 4 kA/m, which is well below their saturation magnetization. Estimation of transition temperature for samples annealed at 573 and 673 K has been done by fitting Curie–Wiess law (insets of figure 7(a, b)) and for samples annealed at 773, 873, 973 and 1073 K by extrapolating the linear section of the M vs T curve to the temperature axis. Magnetization of the sample annealed at 773 K with particle size 8 nm exhibits a steady decrease with an increase in the temperature and changes its curvature around T_C (figure 8). On the other hand, magnetization of samples annealed at 873, 973 and 1073 K with particle size of 19, 33 and 40 nm, respectively, reach a maximum at T_{max} and then decreases abruptly with further increase in temperature.

Figure 9 shows the plot of the variation of transition temperature vs particle size of the $Cu_{0.25}Co_{0.25}Zn_{0.5}Fe_2O_4$ particles annealed at different temperatures from which it is clear that there is a smooth decrease in the transition temperature with decrease in particle size. The decrease is significant below 8 nm. As the cation distribution is the same for samples annealed at different temperatures (tables 3 and 4), the decrease in Curie temperature with decrease in the particle size could be due to finite size scaling or a surface effect. The finite size scaling theory predicts the shift of Curie temperature vs particle size by the following equation (Binder 1972)

$$\frac{T_C(\infty)-T_C(d)}{T_C(\infty)}=\left(\frac{d}{d_0}\right)^{-1/\nu}, \tag{3}$$

where $T_C(d)$ is the Curie temperature of the particle having size d, $T_C(\infty)$ the Curie temperature of the bulk, d_0 is the constant representing the microscopic dimensions and ν is the critical exponent of the correlation length.

It is also possible that T_C decreases due to some unknown surface effect. For small particles, a significant

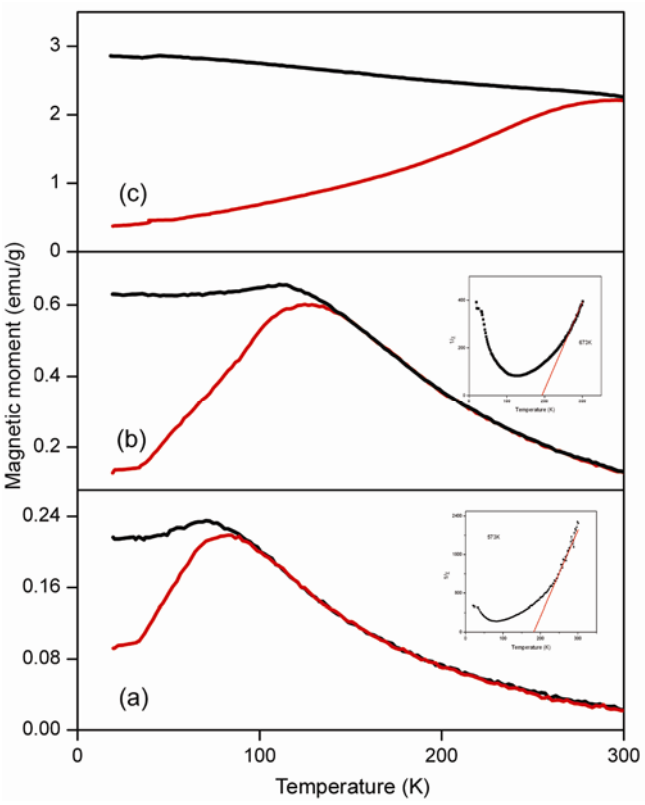

Figure 7. FC–ZFC measurements for the samples annealed at: (**a**) 573, (**b**) 673 and (**c**) 773 K.

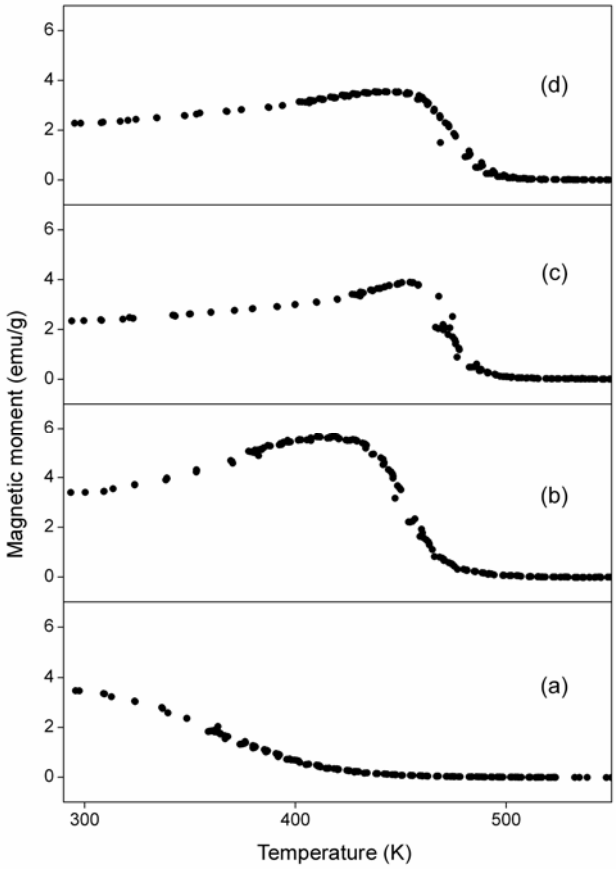

Figure 8. High temperature M–T measurements for samples annealed at: (**a**) 773, (**b**) 873, (**c**) 973 and (**d**) 1073 K.

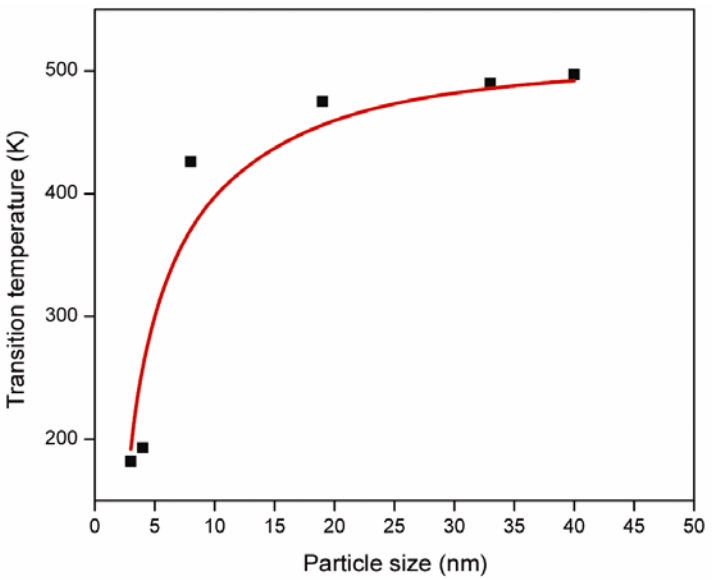

Figure 9. Transition temperature as function of particle size. The solid line is the fit of experimental data with (3).

fraction of atoms is on the surface and it is reasonable to expect their magnetic interaction to be different, leading to a different average Curie temperature. Since the ratio of surface to bulk atoms in a particle is proportional to d^{-1}, such an effect, if linearly dependent on the specific surface area, might yield a change in T_C proportional to d^{-1}, which would be mathematically equivalent to (3) with $\nu = 1$ (Tang *et al* 1992).

The variation of the transition temperature with particle size is very well reproduced on fitting the experimental data (red line in figure 9) with (3) upon which we obtain T_C $(\infty) = 515$ K, $d_0 = 1{\cdot}9$ nm and $\nu = 0{\cdot}98$. The value of d_0 indeed represents a microscopic dimension that is approximately twice the lattice constant of the particles. The value of ν, obtained from the fitting, shows that the decrease in the Curie temperature (T_C) with decrease in particle size of $Cu_{0{\cdot}25}Co_{0{\cdot}25}Zn_{0{\cdot}5}Fe_2O_4$ is consistent with the finite size scaling theory.

4. Conclusions

This study on $Cu_{0{\cdot}25}Co_{0{\cdot}25}Zn_{0{\cdot}5}Fe_2O_4$ nanoparticles prepared by a simple co-precipitation technique shows that single-phased ferrite nanoparticles with varying particle sizes obtained by controlling the annealing temperature exhibit interesting size effects. The presence of a magnetically dead surface layer leads to an increase in the effective anisotropy constant. The saturation magnetization and coercivity also show size dependence. FC–ZFC studies show evidence for inter-particle interactions and the decrease of T_C with particle size is consistent with finite size scaling theory.

References

Ai L and Jiang J 2010 *Curr. Appl. Phys.* **10** 284
Andrés Vergés M, Costo R, Roca A G, Marco J F, Goya G F, Serna C J and Morales M P 2008 *J. Phys. D: Appl. Phys.* **41** 134003
Berkowitz A E, Schuele W J and Flanders P J 1968 *J. Appl. Phys.* **39** 1261
Binder K 1972 *Physics* **62** 508
Caizer C and Stefanescu M 2002 *J. Phys. D: Appl. Phys.* **35** 3035
Chinnasamy C N, Jeyadevan B, Shinoda K, Tohji K, Djayaprawira D J, Takahashi M, Justin R Joseyphus and Narayanasamy A 2003 *Appl. Phys. Lett.* **83** 2862
Choudhari A, Mandal M and Mandal K 2009 *J. Alloys Compd.* **48** 7698
Coey J M D 1971 *Phys. Rev. Lett.* **27** 1140
Coey J M D and Khalafella K 1972 *Phys. Status Solidi.* **A11** 229
Costa A C F M, Tortella E, Morelli M R and Kiminami R H G A 2003 *J. Magn. Magn. Mater.* **256** 174
Dennis C L, Jackson A J, Borchers J A, Hoopes P J, Strawbridge R, Foreman A R, Van Lierop J, Grüttner C and Ivkov R 2009 *Nanotechnology* **20** 395103
Gajbhiye N S, Balaji G and Ghafari M 2002 *Phys. Status Solidi* **A189** 357
Garcia del Muro M, Batlle X and Labarta A 1999 *Phys. Rev.* **B59** 13584
Hassnain J G, Rizwan A S, Hasanain S K, Güntherodt G and Ismat S 2010 *J. Appl. Phys.* **108** 063921
Hiroi K, Komatsu K and Sato T 2011 *Phys. Rev.* **B83** 224423
Hu H, Tian Z, Liang J, Yang H, Dai A, An L, Wu H and Yang S 2011 *Nanotechnology* **22** 085707
Jeun M, Lee S, Kyeong Kang J, Tomitaka A, Wook Kang K, Ii Kim Y, Takemura Y, Chung K W, Kwak J and Bae S 2012 *Appl. Phys. Lett.* **100** 092406

Kihal A, Fillion G, Bouzabata B and Barbara B 2012 *Phys. Status Solidi* **B249** 604

Kodama R H, Berkowitz A E, McNiff Jr E J and Foner S 1996 *Phys. Rev. Lett.* **77** 394

Krieble K, Schaeffer T, Paulsen J A, Ring A P, Lo C C H and Snyder J E 2005 *J. Appl. Phys.* **97** 10F101

Kumar V, Ranaa A, Yadav M S and Pant R P 2008 *J. Magn. Magn. Mater.* **320** 1729

Lakshmi N, Bhargava H, Suwalka O P, Venugopalan K, Reddy V R and Gupta A 2009 *Phys. Rev.* **B80** 174425

Lima E, De Biasi E, Mansilla M V, Saleta M E, Effenberg F, Rossi L M, Cohen R, Rechenberg H R and Zysler R D 2010 *J. Appl. Phys.* **108** 103919

Mørup S, Hansen M F and Frandsen C 2010 *Beilstein J. Nanotechnol.* **1** 182

Roy S, Dubenko I, Eddorh D D and Ali N 2004 *J. Appl. Phys.* **96** 1202

Sharma S K, Kumar R, Kumar S, Knobel M, Meneses C T, Sivakumar V V, Reddy V R, Singh M and Lee C G 2008 *J. Phys. Condens Matter.* **20** 235214

Šutka A, Pärna R, Zamovskis M, Kisand V, Mezinskis G, Kleperis J, Maiorov M and Jakovlev D 2013 *Phys. Status Solidi* doi: 10.1002/pssa.201329039

Sawatzky G A, Van Der Woude F and Morrish A H 1969 *Phys. Rev.* **187** 747

Sindhu S and Birajdar D D 2013 *IOSR J. Appl. Phys.* **3** 33

Tailhades Ph, Villette C, Rousset A, Kulkarni G U, Kannan K R, Rao C N R and Lenglet M 1998 *J. Solid State Chem.* **141** 56

Tang Z X, Chen J P, Sorensen C N, Kalabunde K J and Hadjipanayis G C 1992 *Phys. Rev. Lett.* **68** 3114

Tang Z X, Sorensen C N, Kalabunde K J and Hadjipanayis G C 1991 *Phys. Rev. Lett.* **67** 3602

Thakur A, Thakur P and Hsu J H 2012 *J. Appl. Phys.* **111** 07A305

Tiwari S D and Rajeev K P 2005 *Phys. Rev.* **B72** 104433

Upadhyay C 2003 Ph D thesis (submitted to IIT Kanpur)

Vázquez-Vázquez C, López-Quintela M A, Buján-Núñez M C and Rivas J 2010 *J. Nanopart. Res.* **13** 1663

Yamamoto Y and Makino A 1994 *J. Magn. Magn. Mater.* **133** 500